Statistical light-mode dynamics of multipulse passive mode locking

Rafi Weill, Boris Vodonos, Ariel Gordon, Omri Gat, and Baruch Fischer
Department of Electrical Engineering, Technion, Haifa 32000, Israel
(Received 28 February 2007; published 11 September 2007; publisher error corrected 1 November 2007)

We study the multipulse formation in passive mode locking in the framework of the statistical light-mode dynamics theory. It is a many-body theory that treats the complex many-mode laser system by statistical mechanics. We give a detailed theory and experimental verification for the important case of multiple-pulse formation in the laser cavity. We follow and extend our former work on the subject. We give a detailed analysis with a rigorous calculation of the partition function, the free energy, and the order parameter in the coarse-graining method within the mean-field theory that is exact in the light-mode system. The outcome is a comprehensive picture of multipulse formation and annihilation, pulse after pulse, in an almost quantized manner, as the noise ("temperature") or the light power is varied. We obtain the phase diagram of the system, showing a series of first-order phase transitions, each belonging to a different number of pulses. We also study the hysteresis behavior, typical for such thermodynamic systems. We elaborate on the role of the saturable absorber structure in determining the multipulse formation. The theoretical results are compared to experimental measurements that we obtained with mode-locked fiber lasers, and we find an excellent agreement.

DOI: 10.1103/PhysRevE.76.031112 PACS number(s): 05.70.Fh, 42.55.Ah, 42.65.−k

I. INTRODUCTION

When the light intensity of passively mode-locked lasers is raised by increasing the pumping rate, the lasing is often characterized by the formation of more than one pulse per cavity round trip [1]. That is, at any given instant, the optical energy is sharply concentrated around several points along the cavity rather than at one point in a single-pulse regime, or evenly distributed over the cavity in a continuous wave (cw) operation. The phenomenon is observed in lasers with different types of saturable absorbers (SA's), regardless of their specific mechanism. However, the modeling of these absorbers can be rather complex and requires the inclusion of high-order nonlinearities [2–7]. In additive pulse mode locking (APM) [8], the transmissivity has an even more complex behavior. It has an oscillatory dependence on pulse input energy, being based on interferometric conversion of the phase difference between two paths or polarizations to an amplitude modulation. Commonly used techniques of this type are nonlinear polarization evolution (NPE) [9,10], nonlinear optical loop mirrors (NOLM's) [11], and their variants.

A remarkable property often observed in multipulse operation is the quantization of the pulse energies [2,12,13]. That is, all pulses possess nearly fixed energy, which is almost independent of, for example, the pumping power. These pulse quanta can move, one with respect to others, attracting or repelling each other, and sometime form ordered structures, such as couples or bunches. These phenomena have been lately receiving increasing attention [14–21].

In several recent papers we presented a new statistical mechanics approach for the many-mode laser [22–32]. This statistical light-mode dynamics (SLD) theory revealed the deep meaning of *noise*, which must be viewed in such many-mode systems as an additional dimension, similar to temperature in thermodynamic systems. Noise is essential for the description of mode locking, and it has to be taken into account *nonperturbatively*, even when it is seemingly weak. The mode system is treated as a many-body system, where the laser modes are the degrees of freedom. Then, understanding the mode system would need a thermodynamicslike approach, and quantities such as the free energy and entropy are essential. An important outcome is that passive mode locking is a first-order phase transition occurring when the noise ("temperature") or the light power is varied. It inherently explains the power threshold needed for passive mode locking.

We applied the SLD theory to the problem of multipulse formation, and preliminary results have been published in a previous Letter [26]. The main finding [26] was that multipulse passive mode locking is well described as a thermodynamiclike system with phases differing by the number of pulses. Formation and annihilation of laser light pulse quanta occur in thermodynamiclike pathway. In the P-T plane (P is the intracavity power and T is the noise strength), the phases are separated by lines of first-order phase transitions, as shown below in Fig. 4.

In this paper, we give a detailed study of the multipulse statistical mechanics system, put the results of [26] on firm foundations with a rigorous statistical mechanics analysis, and also extend it and present several new results. The new aspects include a detailed understanding of the validity of the coarse-graining and the mean-field theory. We also elaborate on the role of the saturable absorber function and the way its oscillatory behavior guarantees multipulse formation.

The statistical mechanics analysis is based on an effective model of the laser dynamics, where the power of the cavity electric field in an interval, whose length is of the order of the pulse width, is represented by a single degree of freedom. (See Ref. [27] for an example of this approach.) The effective model is derived in Sec. II. It gives the actual laser overall dynamics in a similar way to that of the Ising model and ferromagnets [33], containing the essential physics of the system under study, rather than using the dynamics of the individual degree of freedom. It is therefore more amenable

to theoretical analysis. The crucial ingredient in the effective model is the transmissivity function s, whose form determines the multipulse properties of the laser. We therefore show (Sec. II B) how s can be derived from the properties of the saturable absorber, and calculate explicit examples for APM and similar types of saturable absorbers, which are compatible with the results of [34,35]. We discuss the properties of s, and find their effect on the pulse properties.

The stochastic equations of the effective model are analyzed using the Fokker-Planck equation formalism, which has provided many theoretical predictions regarding laser light (in single-mode lasers) [36–38]. The analysis shows [22,23] that the equations obey the potential condition [38], and the steady state measure is, therefore, immediately identified as the Gibbs distribution of an effective "Hamiltonian" at temperature T. The analysis then proceeds along the standard route of calculating the free energy F, from which all steady state properties follow. As shown in [26], the model can be studied using mean-field-like methods, which become exact in the thermodynamic limit, where the ratio of the cavity length to the pulse width tends to infinity. This calculation is carried out in detail in Sec. III, where F is shown to be the minimum of a Landau function f, which depends on a multicomponent order parameter, whose components are the pulse powers. The study of the structure of f and the dependence on the system parameters P and T yields all desired information on the steady state properties of the laser and its phase diagram. The behavior is particularly simple at high pumping rate, where the intracavity power is much larger than the typical pulse power.

For the experimental part, we describe in Secs. IV and V the fiber laser system that was used to study the multipulse mode-locking behavior. The saturable absorber part for the passive mode locking is obtained in the fiber by NPE, to which the present theory applies. The laser is supplied with an external noise source; so both P and T are experimentally tunable.

Then we proceed in Sec. V with theoretical results, which are compared to the experiment regarding basic measured thermodynamic properties. We first find the phase diagram, which is shown to have phases differing by the number of pulses. In the P-T plane the phases are separated by lines of first-order phase transitions, signifying abrupt creation or annihilation of a single pulse. Then we give the calculation and experimental measurements of the order parameter and the pulse energy as a function of the noise strength T. Experimental phase diagrams and hysteresis curves are produced, showing remarkable agreement with the theoretical predictions.

We also touch on the hysteresis behavior of the system analyzed and observed in the experiment. Here, we need to study the properties of the metastable states given by the free energy. Since, as shown, typical barrier heights between metastable and stable states are much larger than the "temperature," the lifetimes of the metastable states are long, virtually infinite, and strong hysteresis is observed. Using the Arrhenius formula, hysteresis curves are derived which agree excellently with experiments.

In the Appendix, a transfer matrix method is used, generalizing our former work [27], to study the system when the number of active modes is large but finite, showing, in particular, that mean-field theory becomes exact in the thermodynamic limit.

II. THE THEORETICAL MODEL

The dynamics of the slowly varying envelope ψ of the cavity (of length L) electric field over many round-trip times is governed by the master equation [8,39]

$$\frac{\partial\psi(z,t)}{\partial t} = \hat{F}[\psi]\psi(z,t) + \Gamma(z,t) = \left(g[\psi(z,t)] + (\gamma_g + i\gamma_d)\frac{\partial^2}{\partial z^2} + \tilde{s}(|\psi(z,t)|^2) + i\gamma_k|\psi(z,t)|^2 \right)\psi(z,t) + \Gamma(z,t). \quad (1)$$

Here z is the spatial coordinate along the cavity, which is bounded at $0<z<L$, and t is a long scale time variable defined over multiple round-trip times. The refractive terms in the net gain functional $\hat{F}$ are the chromatic dispersion and Kerr effect, characterized by the coefficients γ_d and γ_k, respectively, and the gain and loss terms are the spectral filtering with coefficient γ_g, the fast saturable absorber characterized by the transmissivity function $\tilde{s}(|\psi|^2)$ per round-trip time, and the incremental net gain $\tilde{g}$ per round-trip time, which depends on the entire wave form of ψ rather than its instantaneous value. $\tilde{s}(0)$ is set to zero by including in $\tilde{g}$ the zero-field losses in the saturable absorber. The white noise $\Gamma(z,t)$ stemming from spontaneous emission and other internal or external sources has an essential role. It is a complex white Gaussian noise with covariance

$$\langle\Gamma^*(z,t)\Gamma(z',t')\rangle = 2TL\delta(z-z')\delta(t-t'), \quad (2)$$

where the constant T, measuring the rate of power injection of the noise, is the effective *temperature*.

If written in Fourier (mode) space, Eq. (1) will take the form

$$\dot{a}_m(t) = \hat{\mathcal{F}}[a]_m + \tilde{\Gamma}_m \quad (3)$$

where $\psi(z,t)=\Sigma_m a_m(t)\exp\left(i\frac{2\pi mz}{L}\right)$, and $\hat{\mathcal{F}}[a]$ is the Fourier representation of $\hat{F}[\psi]\psi(z,t)$ containing terms which are coupled coherently to the mth mode a_m. The covariance of the noise is now

$$\langle\tilde{\Gamma}_m^*(t)\tilde{\Gamma}_n(t')\rangle = 2T\delta_{m,n}\delta(t-t'). \quad (4)$$

In the literature the transmissivity function is often approximated by its linear behavior near zero field, $\tilde{s}(|\psi|^2) \sim \gamma_s|\psi|^2$, which is appropriate when pulses are weak. Here, we study the case where pulses are strong and the entire functional form of $\tilde{s}$ has to be taken into account.

In ultrafast optics it is often the case that the dispersive terms in Eq. (1) (chromatic dispersion and Kerr effect) are much stronger than all others. Then pulses are well modeled by nonlinear-Schrödinger-equation solitons:

$$\psi_s(z,t) = A_0\,\mathrm{sech}\left(\frac{z}{z_p}\right)\exp\left(-i\frac{|\gamma_d|}{z_p^2}t\right), \quad (5)$$

where the amplitude A_0 and pulse width z_p are related by the soliton area relation

$$A_0^2 z_p^2 = 2\frac{|\gamma_d|}{\gamma_k} \equiv \frac{B}{2}.$$

The soliton power is $2A_0^2 z_p = B/z_p$, and is determined dynamically, as discussed below.

A. The coarse-grained master equation

In order to facilitate the analysis, we proceed to construct an effective master equation motivated by the energy rate analysis that was developed in [5]. There, a rate equation for the pulse or cw energy is constructed from Eq. (1) by integrating over the whole cavity duration under the assumption that the laser is operating either in pulses or in cw mode. In our study, we construct *local* rate equations for the power in a short cavity interval.

Consider a cavity of a passively mode locked laser sampled at constant times in each round trip. If mode locking has occurred, one or more pulses occupy short cavity intervals, but the optical signal pervading most of the intervals is a noise-generated cw. To describe such a hybrid state, the cavity is divided into N intervals, whose size Δ is chosen to be large enough to completely contain a short stable pulse. N must be chosen to equal the number of active modes in the cavity [40], and in multimode lasers it is much larger than 1.

A rate equation is constructed to describe the energy in each of the intervals, whether it contains a pulse or cw background. In this way, the energy of the continuum is not represented by a single degree of freedom as in [5], but by many. We will show that when noise is present the continuum carries essentially all the entropy [27], and hence it is crucial that it is represented by many degrees of freedom.

From Eq. (1) and its complex conjugate we derive the rate equation for the energy

$$x_m(t) = \int_{m\Delta}^{(m+1)\Delta} |\psi(z,t)|^2 dz' \tag{6}$$

in an interval $m=1,\ldots,N$, under the assumption that there is no overlap of intervals:

$$\frac{\partial}{\partial t} x_m = 2\,\mathrm{Re}\int_{m\Delta}^{(m+1)\Delta} [\psi^* \hat{F}(\psi)\psi + \psi^* \Gamma(z',t)] dz'. \tag{7}$$

The right-hand side of the last equation contains two terms that need evaluation. To evaluate the first, we assume that the form of ψ belongs to a one-parameter set of functions [for example, the soliton function (5)], and that the interaction between different intervals is weak enough that there is no coupling between the intervals; then the integration can be carried out, and the first term can be rewritten as $s(x_m)x_m + g(\Sigma x_i)x_m$. $s(x)$ is the effective nonlinear gain for the energy in the interval (which depends on $\tilde{s}$ but also on the parabolic gain, Kerr effect, etc.) and g is the overall net gain (originating from the slow amplifier and effective linear losses). By properly modifying g, one can always set $s(0)=0$.

The second term contains the noise, and is evaluated by calculating the corresponding noise-induced drift $D_{m,noise\text{-}ind}$ (which is the part of the drift coefficient D_m that stems from the noisy term) and the diffusion matrix $D_{m,n}$ of the Fokker-Planck equation (see [38]).

$$D_{m,noise\text{-}ind} = \lim_{\tau\to 0} \frac{1}{\tau}\left\langle \int_t^{t+\tau} 2 \times \mathrm{Re}\int_{m\Delta}^{(m+1)\Delta} \psi^*(z',t')\Gamma(z',t')dt'dz' \right\rangle, \tag{8}$$

$$D_{m,n} = \lim_{\tau\to 0} \frac{1}{\tau}\left\langle \left(\int_t^{t+\tau} 2\,\mathrm{Re}\int_{m\Delta}^{(m+1)\Delta} \psi^*(z',t')\Gamma(z',t')dz' \right) \times \left(\int_t^{t+\tau} 2\,\mathrm{Re}\int_{n\Delta}^{(n+1)\Delta} \psi^*(z',t')\Gamma(z',t')dz' \right) \right\rangle. \tag{9}$$

The noise-induced drift is calculated with the aid of the Fourier representation of the wave envelope and the noise [Eqs. (3) and (4)]:

$$\begin{aligned} &2\,\mathrm{Re}\int_{m\Delta}^{(m+1)\Delta} \psi^*(z',t')\Gamma(z',t)dz' \\ &= 2\,\mathrm{Re}\int_{m\Delta}^{(m+1)\Delta} \sum_{m,l}^{N} a_m^*(t')\tilde{\Gamma}_l(t')\exp\left(i\frac{2\pi(l-m)z}{L}\right)dz' \\ &= 2\,\mathrm{Re}\int_t^{t'}\int_{m\Delta}^{(m+1)\Delta} \sum_{m,l}^{N} [\hat{\mathcal{F}}[a]_m^* + \tilde{\Gamma}_m^*(t'')]\Gamma_l(t') \\ &\quad\times \exp\left(i\frac{2\pi(l-m)z}{L}\right)dz'dt''. \end{aligned} \tag{10}$$

Taking the average will result simply in $2NT\Delta = 2TL$.

The diffusion coefficient is calculated in a straightforward manner, and the resulting coefficients finally take the forms

$$D_m = s(x_m)x_m + g\left(\sum x_i\right)x_m + 2TL, \tag{11}$$

$$D_{m,n} = 2TLx_m\delta_{m,n}. \tag{12}$$

An energy rate equation equivalent to Eq. (7) can be written, which leads to the same drift and diffusion coefficients:

$$\frac{dx_m}{dt} = s(x_m)x_m + g\left(\sum x_i\right)x_m + 2TL + \sqrt{x_m}\Gamma_m(t). \tag{13}$$

The Γ_m are independent real Gaussian white noise processes satisfying $\langle \Gamma_m(t)\tilde{\Gamma}_n(t')\rangle = 4TL\delta_{m,n}\delta(t-t')$, and the last term multiplying the noise is in the Ito interpretation [38].

We will now derive the form of s under the assumption that the refractive parts (Kerr effect and dispersion) in Eq. (1) are much larger than the other terms, and therefore the pulses have the solitonic form of Eq. (5) and only their energy is determined from the gain and loss. In this case, because the pulse is not chirped, the refractive terms do not contribute to the integration in (7), and if a pulse occupies the mth interval, its energy x_m can be represented in terms of the pulse duration by $x_m = B/z_p$. The rate equations then take the form (13) with

$$s(x_m) = \frac{2}{x_m}\left(\int_{m\Delta}^{(m+1)\Delta} \tilde{s}(|\psi_s|^2)|\psi_s|^2 dz' - \frac{\gamma_g x_m^3}{6B^2}\right), \quad (14)$$

which can be expressed by means of z_p and hence by x_m. When x_m is small, $s(x_m)$ tends to zero, as is appropriate in the case that the mth interval belongs to the continuum.

We assume that the interaction between different intervals is weak enough that the equations of motion for the x_m's are not coupled, other than through the gain term g. The gain term is responsible for maintaining a mean power $\mathcal{P} = \Sigma_{m=1}^{N} x_m$ inside the cavity. This power is determined by the pumping by stimulated emission. It was shown in [27] that, once $\mathcal{P}$ is given, the specific form of g is unimportant in the thermodynamic limit, $N \to \infty$; this result can be phrased as a statement of equivalence of statistical ensembles, the fixed energy and the variable energy ensembles. In the analysis here we therefore impose a constraint of fixed power $\mathcal{P}$, simplifying the calculation without any loss of generality. g becomes then a Lagrange multiplier for the power constraint

Equation (13) is the coarse-grained master equation. Since it satisfies the potential condition [38], the steady state distribution is

$$\rho(x_1, \ldots, x_N) = \frac{1}{\mathcal{Z}_N} e^{-\mathcal{H}(x_1,\ldots,x_N)/2T} \delta\left(\mathcal{P} - \sum_{m=1}^{N} x_m\right). \quad (15)$$

This is the statistical mechanics Gibbs distribution for the Hamiltonian

$$\mathcal{H}(x_1, \ldots, x_N) = -L \sum_{m=1}^{N} S(x_m), \quad S(x) = \int^{x} s(x')dx', \quad (16)$$

and $\mathcal{Z}_N$ is the corresponding partition function. In Sec. III, we analyze this distribution using tools from statistical mechanics, but first we study the properties of the effective nonlinear gain function $s(x)$.

B. Nonlinear saturable absorber

The purpose of this section is to show different transmissivity functions $\tilde{s}$ derived in the past, where the saturation deviates from the standard linear dependence on intensity. The resulting form of $s(x)$, the effective nonlinear gain, has a major effect on the mode-locking behavior, as we find below. In this section we obtain specific examples of $s(x)$, while in the rest of the paper we keep the discussion as general as possible in regards to s.

In general, the transmissivity depends on the exact method of the saturable absorber used for mode-locking. In the NOLM method [11]

$$\tilde{s}(|\psi|^2) = \frac{1}{2}\left[1 - q\cos\left(\frac{\pi|\psi|^2}{I_{sat}} + \phi_0\right)\right], \quad (17)$$

where q is the modulation depth, ϕ_0 accounts for linear bias, and I_{sat} is the saturation intensity. Other methods of APM, such as the polarization rotation technique (used in our experiments), are described by more complex models, but eventually they have an oscillating form which resembles the one introduced in the equation above (see, for example, [10]).

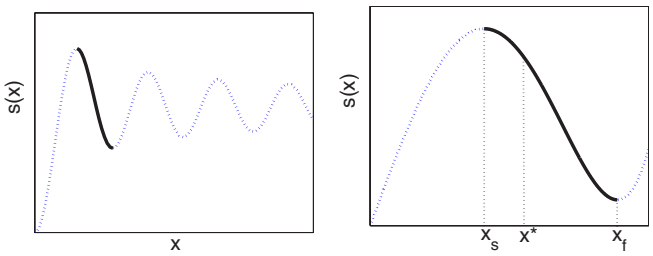

FIG. 1. (Color online) Left: The effective nonlinear gain function calculated numerically from Eq. (14) with the transmissivity (17) ($q=0.8$, $\phi_0=\gamma_g=0$). Right: A polynomial fit $s(x)=ax^2-bx^3+cx^4$. The figure shows the points x_s, x_f, x^*, the first maximum, second minimum, and asymptotic pulse strength, respectively, and the active region, bold black, for the multiple-pulse regime.

The effective nonlinear gain can be calculated numerically using Eq. (14) for solitonic shaped pulses, and the outcome is an oscillatory function with exponentially decaying oscillations [34,35], as seen in Fig. 1. The same behavior has been measured experimentally by injecting soliton pulses with different energies into the loop and measuring their output energy [34]. We note that the same qualitative structure holds for other pulse forms, and that changing ϕ_0 does not change the behavior either.

It is shown below that, when s is oscillatory, the pulse powers in the multipulse regime always lie in the active interval between x_s, the first maximum of $s(x)$, and x_f, the second minimum, while in the limit of a large number of pulses the pulse powers approach the asymptotic value x^*, given implicitly by $x^* s(x^*) = S(x^*)$ (see Fig. 1). Since it is important to model s accurately only in the active region, we can use a polynomial approximation.

Many previous studies (see, for example, Ref. [39]) concentrated on the weak pulse limit, where $\tilde{s}$ can be approximated by its Taylor expansion near zero intensity:

$$\tilde{s}(|\psi|^2) = \gamma_s |\psi|^2. \quad (18)$$

The effective nonlinear gain for a solitonlike pulse is then

$$s(x) = \frac{1}{3B}\left(2\gamma_s - \frac{\gamma_g}{B}\right)x^2. \quad (19)$$

In this regime mode locking yields a *single* pulse [27], a result that holds in general for monotonic s functions, as we show below.

However, in every physical laser system $\tilde{s}$ must saturate (or oscillate). Equation (19) then tells us that s can no longer be monotonic due to the spectral filtering; hence, breakup of pulses will always occur.

III. MEAN-FIELD CALCULATION OF THE FREE ENERGY

A. The partition function

Since the steady state distribution of the energy variables x_m is an equilibrium distribution [Eq. (15)], we carry out the analysis by calculating the partition function $\mathcal{Z}_N$, obtained by

integrating over all possible x configurations,

$$\mathcal{Z}_N(\mathcal{P},T)=\int [dx]\exp\left(\frac{1}{2T}\sum_{i=1}^{N}S(x_i)\right)\delta\left(\sum_{i=1}^{N}x_i-\mathcal{P}\right), \tag{20}$$

where $[dx]$ denotes integration with respect to all x's from zero to infinity.

Because of the power constraint, the amplitude of x at most sites is $O(1/N)$, for which the effective nonlinear gain is negligible. These sites will be referred to as the *continuum*. We now make the assumption that the main contribution to $\mathcal{Z}_N$ comes from configurations where at most a finite number m of x variables are $O(1)$, i.e., pulses, while the rest are $O(1/N)$. This assumption, which allows for the calculation of the free energy by mean-field methods, is justified by the rigorous calculations in the Appendix.

This assumption leads to the following calculation:

$$\begin{aligned}\mathcal{Z}_N(\mathcal{P},T)&\sim\int\prod_{i=1}^{m}dx_i\exp\left(\frac{1}{2T}\sum_{i=1}^{m}S(x_i)\right)\\&\times\int\prod_{i=m+1}^{N}\delta\left(\sum_{i=m+1}^{N}x_i-\left(\mathcal{P}-\sum_{i=1}^{m}x_i\right)\right)\\&\propto\int\prod_{i=1}^{m}dx_i\exp\left\{-N\left[-\frac{1}{2NT}\sum_{i=1}^{m}S(x_i)\right.\right.\\&\left.\left.-\ln\left(\mathcal{P}-\sum_{i=1}^{m}x_i\right)\right]\right\}.\end{aligned} \tag{21}$$

In order to evaluate the last integral in Eq. (21), we use the saddle point approximation. As $N\to\infty$, the main contribution to the integral is from the global minimum of the thermodynamic potential

$$f_m(x_1,\ldots,x_m)=-\frac{1}{2NT}\sum_{i=1}^{m}S(x_i)-\ln\left(\mathcal{P}-\sum_{j=1}^{m}x_j\right). \tag{22}$$

In order to get a nonzero minimizer, $\mathcal{T}\equiv 2NT$ must have a finite limit (we shall see that $\mathcal{T}$ plays the role of temperature in the system and hence it will be referred to as such). The necessity of rendering the parameters in this problem N dependent has been discussed before in [27].

We denote the global minimum of f_m by $F_m(\mathcal{P},\mathcal{T})/\mathcal{T}$. Let n be the smallest m for which the minimum of $F_m(\mathcal{P},\mathcal{T})$ with respect to m is attained, i.e., the minimizer of f_m is $(\bar{x}_1,\ldots,\bar{x}_n,0,\ldots,0)$. Our statement, which will be proven in the Appendix, is that $\mathcal{Z}_N$ takes the asymptotic form

$$\mathcal{Z}_N(\mathcal{P},\mathcal{T})\sim\frac{1}{N!}A_N(\mathcal{P},\mathcal{T})e^{-NF_n(\mathcal{P},\mathcal{T})/\mathcal{T}}, \tag{23}$$

i.e., F_n is the free energy per degree of freedom. Moreover, n is the number of pulses per roundtrip and $\bar{x}_1,\ldots,\bar{x}_n$ are their powers, and $n=0$ corresponds to a cw. Notice that, since equilibrium thermodynamics is applicable, the free energy structure obeys the relation

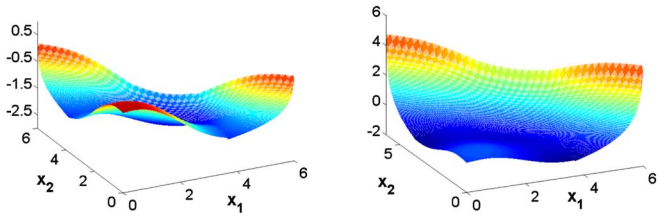

FIG. 2. (Color online) Thermodynamic potential $f_2(x_1,x_2)$. In the right figure, f_2 has local minima at $(X(1),X(0))$, $(0,X(1))$ and (0,0) and a global minimum at $(X(2),X(2))$. In the left figure, the function is plotted for higher temperature; thus its global minima are now at $(0,X(1))$ and $(0,X(1))$. $X(n)$ is given in Eq. (26).

$$F_n(\mathcal{P},T)=\mathbf{E}-\mathcal{T}\mathbf{S}, \tag{24}$$

where $\mathbf{E}=-\Sigma_{i=1}^{n}S(\bar{x}_i)$ is the mean energy per degree of freedom, and $\mathbf{S}=\ln(\mathcal{P}-\Sigma_{i=1}^{n}\bar{x}_i)$ the entropy per degree of freedom.

B. Properties of the thermodynamic potential

Evidently, the thermodynamic potential f_m introduced in Sec. III A is the crucial part that determines the thermodynamics. Here, we analyze this function and study its general properties. By making a plausible assumption, the structure of f can also be used to study dynamic properties, such as hysteresis.

An example of the thermodynamic potential is drawn in Fig. 2 for $m=2$. The optimization problem we need to tackle is to find the global and local minima of f_m subject to the constraints $x_i\geqslant 0$, $\forall i$, and $\Sigma_{i=1}^{m}x_i\leqslant\mathcal{P}$. The global minima will correspond to the stable states and the local ones will correspond to metastable states. We also look for saddle points and local maxima in order to understand the dynamics. These points are permutations of vectors of the form $(y_1,\ldots,y_n,0,\ldots,0)$ (where n can take any value between 0 and m). The y_i's can be found using $\partial_i f_m=0, i\leqslant n$, which leads to the n coupled equations

$$s(y_j)\left(\mathcal{P}-\sum_{i=1}^{n}y_i\right)=\mathcal{T},\quad 0=1,\ldots,n. \tag{25}$$

These equations can be solved easily numerically, given a specific form of s, when n is small, and by substituting the solution into the square matrix of second-order partial derivatives the type of the critical point can also be determined.

As $\mathcal{T}$ and $\mathcal{P}$ are varied the values of f at the minima change, and at some point may exchange stability. The points where the identity of the global minimum is exchanged have the thermodynamic significance of a first-order phase transition. It often happens that the transition involves an increase or decrease in the number n of nonzero x values at the minimizer. Then phases are labeled by the number of pulses. Generically, the points of coexistence form one-dimensional curves in the $\mathcal{T}-\mathcal{P}$ plane. See Fig. 4 for an example of a phase diagram.

In the next section, we describe the multipulse phase diagram for the s that corresponds to the nonlinear SA, but

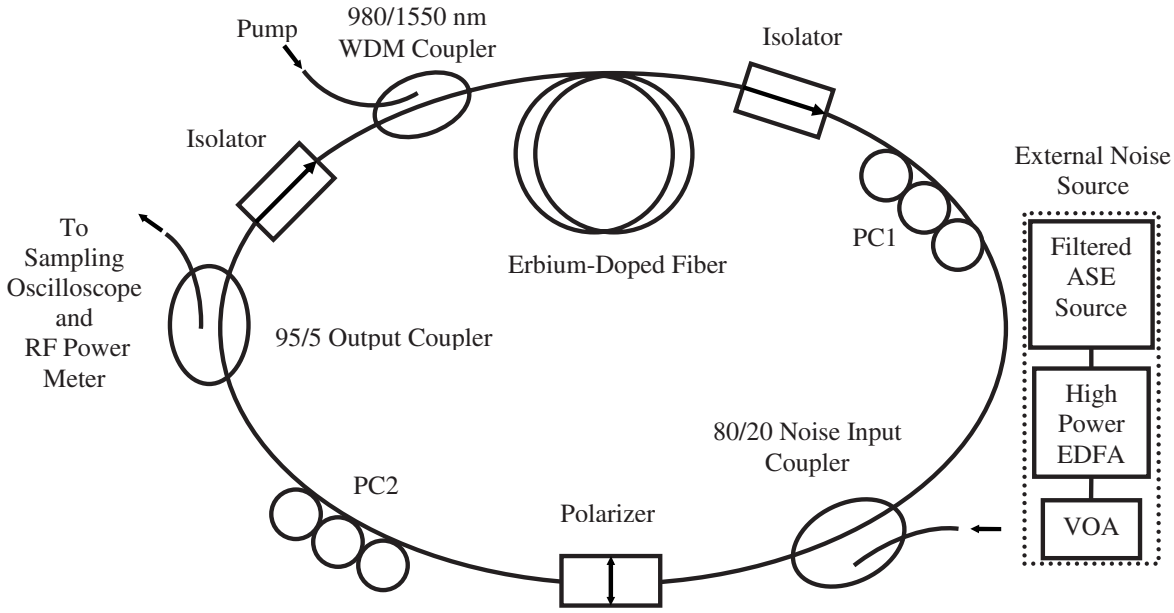

FIG. 3. Schematic of the experimental setup. The fiber ring laser consisted of an erbium-doped fiber amplifier (EDFA) pumped by a 980 nm laser source through a wavelength-division multiplexing (WDM) coupler, isolators that assure oscillations in one direction only, while the polarization controllers (PCs) and the polarizer provide the effective saturable absorber action (by utilizing nonlinear polarization rotation in the fiber cavity). The external noise source for the tunable noise ("temperature") is constructed from a filtered amplified spontaneous emission (ASE) source, high-power EDFA, and variable optical attenuator (VOA).

several interesting properties of the thermodynamics can be deduced on general grounds.

(1) For every positive temperature $\mathcal{T}$, there exists a threshold energy $P_0(\mathcal{T})$ such that for $P<P_0(\mathcal{T})$ the global minimum is the zero configuration, i.e., cw operation.

(2) Furthermore, since $S(x)$ increases more slowly than linearly at $x=0$, the zero configuration is a *local* minimum for any positive $\mathcal{T}$, i.e., the cw state is always metastable. This property explains the "self-starting" threshold [31,32].

(3) As $\mathcal{T}$ increases, the total pulse power $\Sigma_{i=1}^{n}\bar{x}_i$ decreases, causing the continuum power and the entropy to increase.

(4) When s is monotonic, the global minimum of f is never attained for configurations with $n\geqslant 2$, i.e., mode locking can result only with a single pulse.

(5) When $s(x)$ is not monotonic and has a global maximum at the point x_s and a positive minimum at $x_f>x_s$, multipulse operation occurs for sufficiently large $\mathcal{P}$ and low $\mathcal{T}$. In this case, the minimizer of f consists of two possible values of $\bar{x}_i$, one of which is smaller than x_s and occurs at most once, and the other is between x_s and x_f. This is also true for the local minima of f.

An interesting special case is where all the pulse powers are equal, a configuration often observed experimentally (see Sec. V). In this case, the metastable n-pulse configuration takes the form $(X(n),X(n),\ldots,X(n),0,\ldots,0)$, where

$$s(X(n))[P-nX(n)]=\mathcal{T}. \tag{26}$$

For s functions of the form defined in item 5 of the above list, $X(n)$ must lie in the interval $x_s<X(n)<x_f$ if $n\geqslant 2$, and the minimum becomes a saddle when $X(n)$ hits the interval end points. The thermodynamically stable state is obtained by minimizing

$$f_n(X(n),X(n),\ldots,X(n))=-\frac{1}{\mathcal{T}}nS(X(n))-\ln[\mathcal{P}-nX(n)] \tag{27}$$

with respect to n. When $\mathcal{P}$ is much larger than the power of a single pulse, the minimizer approaches x_*, given implicitly by

$$x_*s(x_*)=S(x_*). \tag{28}$$

This result explains the almost constant pulse power observed experimentally in the multipulse regime (see Sec. V). Linearizing Eq. (26) near x_*, it also follows that in the multipulse regime the phase transition curves approach straight lines [26],

$$\mathcal{T}=s(x_*)-(n-1/2)S(x_*), \tag{29}$$

for the transition between $(n-1)$-pulse and n-pulse configurations.

IV. THE EXPERIMENTAL SETUP

The experimental system is schematically described in Fig. 3. It consists of a fiber ring laser with passive mode locking (PML) by the nonlinear polarization rotation technique [9,13]. The external noise source was derived from an amplified spontaneous emission system that was injected into the cavity from an external source. The control of its strength provided the temperature tunability. The laser round-trip time

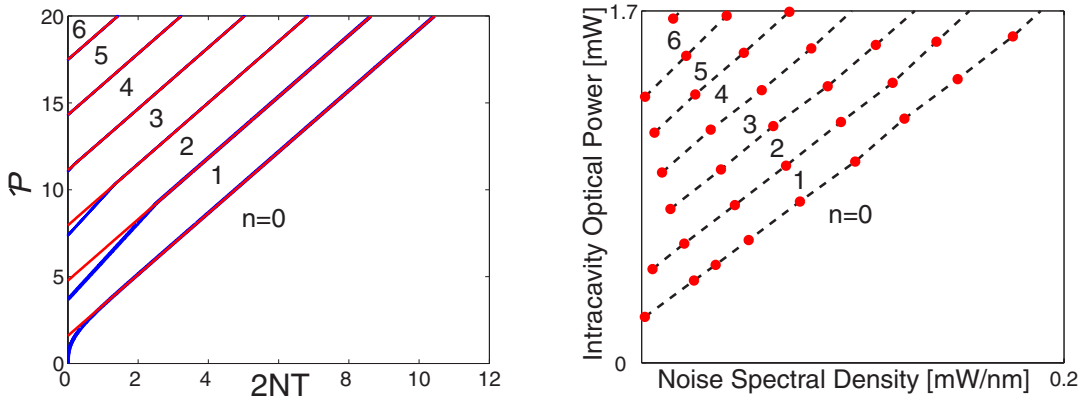

FIG. 4. (Color online) Experimental (right) and theoretical (left) phase diagrams. The theoretical graph shows the number of pulses as a function of the intracavity energy $\mathcal{P}$ and the total noise power $2NT$. The curves of discontinuity have the thermodynamiclike meaning of first-order phase transitions. The straight lines are asymptotes of the transition lines for $\mathcal{P} \gg x_s$ [Eq. (29)].

was 100 ns, corresponding to approximately 20 m of total cavity length, including a 4.3-m-long erbium-doped fiber amplifier with small signal gain of 6 dB/m. The saturable absorber was provided by nonlinear polarization rotation and polarizers, as was formerly described [25,26,29]. By proper adjustment of the polarization controllers (PCs) PML operation was established with generation of subpicosecond pulses. Increasing the pumping power generated multiple pulses in the cavity, a phenomenon that has been frequently observed in a variety of PML fiber lasers [1,9,12,13]. The pulses were often formed in stable bunches with almost equal spacing, which ranged from a few to hundreds of picoseconds, depending on the positions of the PCs, the pumping, and the injected noise level.

As the noise or pumping level was varied, two types of responses of the pulse bunch were observed: variations in the spacing between adjacent pulses and variations in the pulse energy. Therefore, depending on the position of the PCs, three distinct regimes of bunched pulse operation were obtained. The first, and the most common, was the regime where both types of response were observed. In the second regime the multipulse bunch contracted or expanded while pulse energies remained constant, and the third regime was characterized by a fixed bunch pattern while pulse energies were varied.

V. EXPERIMENTAL VS THEORETICAL RESULTS

In this section, we give results of the theoretical analysis regarding thermodynamic features of the multipulse laser system, along with experimental measurements. We show the phase diagrams, the multiphase transition dependence on noise and power, and the hysteresis behavior. The agreement between the theory and the experiment is remarkable; thus showing the power and the validity of the thermodynamic SLD approach.

A. Steady state and phase diagram

We start with the theoretical part, which was performed using the polynomial approximation described above. Figure 4 shows the phase diagram, where each phase is labeled by the number of pulses. The separation lines represent first-order phase transitions. Figure 5 shows the individual pulse power as dashed lines, and the order parameter

$$Q = \sum_{j=1}^{N} \bar{x}_j^2 = nX(n)^2 \tag{30}$$

as a full line, as a function of the noise power. Q is a useful quantity because it is directly proportional to the measured rf power, shown in the experimental graph.

The experimental part of the phase diagram in Fig. 4 was measured as follows. For several pumping powers the injected noise level was raised gradually from zero, the pulses disappeared one by one, and the transition temperatures and average output optical powers were recorded. (Such a behavior was previously observed as the pumping power was decreased [2,13]). The noise spectral density values that were

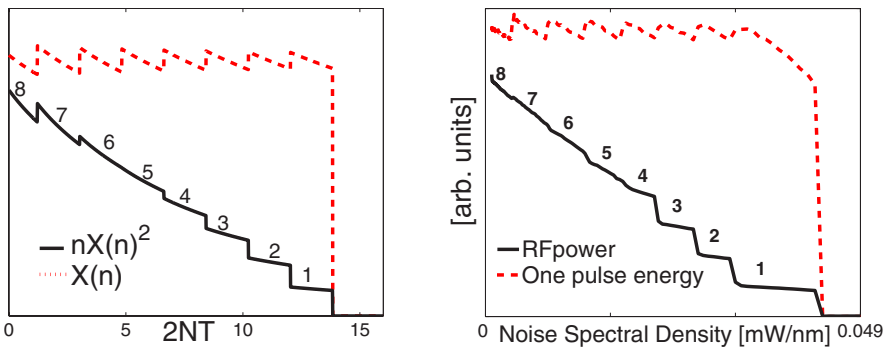

FIG. 5. (Color online) Theoretical (left) and experimental (right) plots of the order parameter $Q=nX(n)^2$ or rf power (solid line) and the mean pulse energy $X(n)$ (dashed line) as functions of the total noise power $2NT$ (proportional to the measured noise spectral density), for a fixed intracavity power.

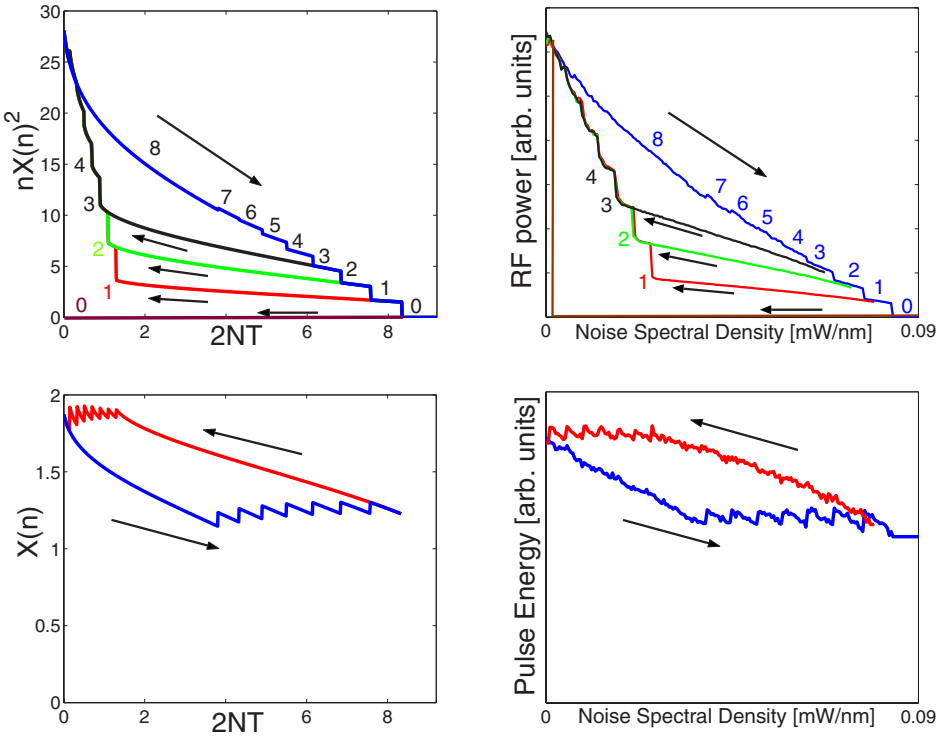

FIG. 6. (Color online) Theoretical (left) and experimental (right) hysteresis curves, showing the order parameter $Q=nX(n)^2$, or rf power (above), and $X(n)$, or pulse power (below), as a function of increasing and decreasing noise levels.

measured by a spectrum analyzer have to be multiplied by 100 to account for the couplers and other internal losses. To obtain the total noise power that perturbs the laser modes ($2NT$ in our theoretical calculations), those measured values also need to be multiplied by the total gain bandwidth of the laser and a coupling factor of the noise power to each cavity mode.

The experimental results presented in Fig. 4 were obtained in the first operation regime, but the structure of the phase diagram was found to be identical in all the regimes mentioned above. Figure 4 demonstrates good agreement between theory and experiment.

The theoretical and experimental plots of the order parameter Q [Eq. (30)] and the energy per pulse as functions of the injected noise level (gradually increased from zero) for a fixed pumping power are shown in Fig. 5. Experimentally, they were obtained by measuring the laser output with a fast photodiode and a rf power meter [25] or a sampling oscilloscope (all having 50 GHz bandwidth), respectively. The pulse energy is nearly constant, with deviations of about 5%. These deviations are well described by the theory. The results of Fig. 5 were obtained in the third operation regime (constant spacing regime described above, where pulse energy changes are most pronounced).

B. Metastable states and hysteresis

Although our mean-field analysis pertains, strictly speaking, only to the steady state, by making a plausible assumption we can use it to study the hysteresis curves of the system—a dynamical property. The free energy is derived from the thermodynamic potential f by saddle point integration, as shown in the Appendix, which receives its dominant contribution from the vicinity of the global minimum. However, the local minima are surrounded by configurations with very small relative probability, so that, if the system is prepared in a configuration corresponding to a local minimum, it may stay trapped there for a very long period; the configuration is metastable. According to the Arrhenius formula, the lifetime of the metastable state is proportional to $\exp(E_b/\mathcal{T})$, where E_b is the height of the potential barrier that separates the metastable state from the stable one. Since the thermodynamic potential is proportional to N, the lifetime diverges as $\exp(N/\mathcal{T})$ in the thermodynamic limit, which means that it becomes very large even for moderate values of N, whereas N in multimode lasers is typically 10^6 or larger. Therefore, a small error is incurred by assuming that the lifetime of a metastable state is infinite, and that the system escapes only when external parameters are changed so as to make the critical point unstable (a saddle or a maximum). An exception to this scenario is the metastable state at zero pulses, i.e., cw operation. This configuration, as shown above, is stable for *any* finite $\mathcal{T}$, so that escape may occur only for very low noise levels. This problem, known as the self-starting problem in passive mode locking, is outside the scope of this paper [31,32].

We now use this argument to compute hysteresis curves for multipulse mode locking under conditions where pulse powers are all equal. As shown above, metastable states are characterized by pulse powers between x_s, the position of the first maximum of s, and x_f, the position of the second minimum. Therefore, on increasing power or decreasing noise level, the pulse powers increase until they reach x_f, and then a new pulse is formed, whereas on decreasing power or increasing noise level, the pulse powers decrease until they reach x_s, and then a pulse is annihilated.

Figure 6 shows theoretical and experimental results for the order parameter Q and the individual pulse power as a

function of noise level. Typically for first-order phase transitions, the system exhibits hysteresis. The number of pulses at any point $(\mathcal{T},\mathcal{P})$ depends on the precise path that led to it. In particular, increasing T leads to a different $Q(T)$ curve than decreasing it. In the T lowering direction, the curves are distinguished by the starting point of the number of pulses. The agreement between theory and experiment is again very good.

VI. CONCLUSIONS

We conclude by noting how powerful the combination of statistical mechanics and laser physics can be, leading to a new view and findings that can be significant to both fields. The many-mode light system is found via the SLD approach to exhibit rich thermodynamiclike behavior with phase transitions, while providing the unique possibility for experimental verification in relatively simple laser systems. The theory was able to explain the basic long-standing question of the mode-locking threshold that is nothing but a first-order phase transition, and many other properties. Very recently, we also showed [29] critical behavior upon adding to the laser external pulses that match the repetition rate of the laser cavity; they act like the external field in magnetic systems or pressure in vapor-liquid-solid systems.

ACKNOWLEDGMENT

This work was supported by the Israel Science Foundation (ISF) founded by the Israeli Academy of Sciences.

APPENDIX: TRANSFER MATRIX CALCULATION

The purpose of this section is to establish Eq. (23) using saddle-point integration. The procedure is a straightforward generalization of that of [27], and is presented in outline. The calculation is based on the recursive version of Eq. (20),

$$\mathcal{Z}_N(\mathcal{P},\mathcal{T}) = \int_0^{\mathcal{P}} dx_1 e^{S(x_1)/\mathcal{T}} \mathcal{Z}_{N-1}(\mathcal{P}-x,\mathcal{T}) \tag{A1}$$

as in [27], and we show that, when N is large, the only significant contribution to the x integration in the last equation comes from the vicinity of a finite set of values of x which maximize the integrand, one of which is $x=0$. The integration on other parts of the interval is exponentially small in N. The case of a single maximizing point will be shown to correspond to invariant measures concentrated on cw configurations where the amplitude of all degrees of freedom is $O(1/N)$. This happens for small enough $\mathcal{P}$ or large T. When there is more than one maximizing point, the typical configurations are such that a finite fraction of the energy is concentrated in a finite number of pulses, while the amplitude of the others is still $O(1/N)$.

Following [27], we study the case of large $\mathcal{T}$ (or small $\mathcal{P}$) by perturbation analysis. $\mathcal{Z}_N^{(0)}(\mathcal{P},\mathcal{T})$ is then determined by the behavior of S for small x, which takes the form γx^k where $k>1$ and γ can also be negative. The perturbative calculation is very similar to the one of Ref. [27], except that here the power k need not be 2, and the result is

$$\mathcal{Z}_N^{(0)} = \frac{P^N}{N!} e^{\xi N^{2-k} P^k}, \quad \xi = \frac{\Gamma(k+1)\gamma}{\mathcal{T}}. \tag{A2}$$

We verify that $\mathcal{Z}_N^{(0)}$ approximates $\mathcal{Z}$ for small enough $\mathcal{P}$ by showing that it solves Eq. (A1) as long as the global minimum $\bar{x}(\mathcal{P},T)$ of the function $f(\mathcal{P},T,x)=-S(x)/\mathcal{T}-\ln(\mathcal{P}-x)$ is zero. As discussed above, for any positive $\mathcal{T}$ there is threshold power $[\mathcal{P}_0(\mathcal{T})]$ below which the global minimum is $\bar{x}=0$. Hence

$$\mathcal{Z}_N(\mathcal{P},\mathcal{T}) = \mathcal{Z}_N^{(0)}(\mathcal{P},\mathcal{T}), \quad \mathcal{P} < \mathcal{P}_0(\mathcal{T}). \tag{A3}$$

Equation (A3) establishes (23) for $\mathcal{P}<\mathcal{P}_0(T)$. We now wish to establish it for arbitrary $\mathcal{P}$. Suppose inductively that (23) holds for $\mathcal{P}<\mathcal{P}_{n-1}(\mathcal{T})$, the power needed to create n pulses at noise level $\mathcal{T}$. Substituting Eq. (23) in Eq. (A1) gives the asymptotic equation

$$\frac{1}{N!} A_N(\mathcal{P},\mathcal{T}) e^{-NF_n(\mathcal{P},\mathcal{T})} \sim \frac{1}{(N-1)!} \int dx\, e^{NS(x)/\mathcal{T}} A_{N-1}(\mathcal{P}-x,\mathcal{T}) \times e^{-(N-1)F_n(\mathcal{P}-x,\mathcal{T})/\mathcal{T}}. \tag{A4}$$

Denoting the part of the exponent proportional to N by $-g$, as before, the integration in (A4) is concentrated near the global minima of g, whose value is

$$\min_x g(\mathcal{P},\mathcal{T},x) \equiv \min_x \frac{-S(x)+F_n(\mathcal{P}-x,\mathcal{T})}{\mathcal{T}} = \min_{x_1,\ldots,x_m} f_m(x_1,\ldots,x_m) = F_n(\mathcal{P},\mathcal{T}). \tag{A5}$$

It is left to show that A_N is subexponential in N. The integration in Eq. (A4) receives its main contributions from the neighborhoods of the minimizers $\bar{x}_i$ of (A5) and from the neighborhood of $x=0$. We denote these contributions by I_i, $i=1,\ldots,m$, and I_0, respectively. The saddle point integration near $x=0$ gives

$$I_0 \sim \frac{1}{(N-1)!} A_{N-1}(\mathcal{P},\mathcal{T}) e^{-(N-1)F_n(\mathcal{P},\mathcal{T})} \int_0^{\mathcal{P}} dx\, e^{-(N-1)|g^{(1)}|x} \sim \frac{e^{F_n(\mathcal{P},\mathcal{T})}}{|g^{(1)}|} \frac{1}{N!} A_N(\mathcal{P},\mathcal{T}) e^{-NF_n(\mathcal{P},\mathcal{T})}, \tag{A6}$$

where we introduced $g^{(1)}=(\partial g/\partial x)|_{x=0}$, which must be negative. The assumption that A_N is subexponential in N was used to approximate $A_{N-1}\sim A_N$. The saddle point integration near $\bar{x}_i$ gives

$$I_i \sim \frac{1}{(N-1)!} A_{N-1}(\mathcal{P}-\bar{x}_i,\mathcal{T}) e^{-(N-1)F_n(\mathcal{P},\mathcal{T})} \times \int_{-\infty}^{\infty} dx\, e^{-(N-1)g_i^{(2)}(x-\bar{x}_i)^2/2} \sim \frac{1}{N!} A_N(\mathcal{P}-\bar{x}_i) \times e^{-NF_n(\mathcal{P},\mathcal{T})} \sqrt{\frac{2\pi(N-1)}{g_i^{(2)}}} e^{F_n(\mathcal{P},\mathcal{T})} \tag{A7}$$

with $g_i^{(2)} = (\partial^2 g/\partial x^2)|_{x\sim\bar{x}_i}$, where $A_{N-1}(\mathcal{P}-\bar{x}_i)$ is associated with configurations with $n-1$ pulses.

Combining these results with Eq. (A4), we get a linear equation for A_N whose solution is

$$A_N(\mathcal{P},\mathcal{T}) = \frac{|g^{(1)}|}{1-e^{F_n(\mathcal{P},\mathcal{T})}} \sqrt{2\pi(N-1)} \sum_i \frac{A_N(\mathcal{P}-\bar{x}_i,\mathcal{T})}{\sqrt{g_i^{(2)}}}. \tag{A8}$$

Using the induction hypothesis, it then follows that $A_N(\mathcal{P},\mathcal{T})$ is indeed subexponential in N, which shows that (23) holds for any $\mathcal{P}$.

[1] D. J. Richardson *et al.*, Electron. Lett. **27**, 1451 (1991).
[2] A. K. Komarov and K. P. Komarov, Phys. Rev. E **62**, R7607 (2000).
[3] N. N. Akhmediev, A. Ankiewicz, and J. M. Soto-Crespo, J. Opt. Soc. Am. B **15**, 515 (1998).
[4] M. J. Lederer *et al.*, J. Opt. Soc. Am. B **16**, 895 (1999).
[5] S. Namiki, E. P. Ippen, H. A. Haus, and C. X. Yu, J. Opt. Soc. Am. B **14**, 2099 (1997).
[6] V. L. Kalashnikov, E. Sorokin, and I. T. Sorokina, IEEE J. Quantum Electron. **39**, 323 (2003).
[7] F. X. Kärtner, J. Aus der Au, and U. Keller, IEEE J. Sel. Top. Quantum Electron. **4**, 159 (1998).
[8] H. A. Haus, IEEE J. Sel. Top. Quantum Electron. **6**, 1173 (2000).
[9] H. A. Haus, E. P. Ippen, and K. Tamura, IEEE J. Quantum Electron. **30**, 200 (1994).
[10] C.-J. Chen, P. K. A. Wai, and C. R. Menyuk, Opt. Lett. **17**, 417 (1992).
[11] M. E. Fermann, F. Haberl, M. Hofer, and H. Hochreiter, Opt. Lett. **15**, 752 (1990).
[12] A. B. Grudinin, D. J. Richardson, and D. N. Payne, Electron. Lett. **28**, 67 (1992).
[13] V. J. Matsas, D. J. Richardson, T. P. Newson, and D. N. Payne, Opt. Lett. **18**, 358 (1993).
[14] J. N. Kutz, B. C. Collings, K. Bergman, and W. H. Knox, IEEE J. Quantum Electron. **34**, 1749 (1998).
[15] A. N. Pilipetskii, E. A. Golovchenko, and C. R. Menyuk, Opt. Lett. **20**, 907 (1995).
[16] A. B. Grudinin and S. Gray, J. Opt. Soc. Am. B **14**, 144 (1997).
[17] D. Y. Tang, B. Zhao, D. Y. Shen, C. Lu, W. S. Man, and H. Y. Tam, Phys. Rev. A **66**, 033806 (2002).
[18] Ph. Grelu, B. Belhache, F. Gutty, and J.-M. Soto-Crespo, Opt. Lett. **27**, 966 (2002).
[19] N. H. Seong and Dug Y. Kim, Opt. Lett. **27**, 1321 (2002).
[20] F. Gutty *et al.*, Electron. Lett. **37**, 745 (2001).
[21] J.-M. Soto-Crespo, N. Akhmediev, Ph. Grelu, and B. Belhache, Opt. Lett. **28**, 1757 (2003).
[22] A. Gordon and B. Fischer, Phys. Rev. Lett. **89**, 103901 (2002).
[23] A. Gordon and B. Fischer, Opt. Commun. **223**, 151 (2003).
[24] A. Gordon and B. Fischer, Opt. Lett. **28**, 53 (2003).
[25] A. Gordon, B. Vodonos, V. Smulakovski, and B. Fischer, Opt. Express **11**, 3418 (2003).
[26] B. Vodonos, R. Weill, A. Gordon, A. Bekker, V. Smulakovsky, O. Gat, and B. Fischer, Phys. Rev. Lett. **93**, 153901 (2004).
[27] O. Gat, A. Gordon, and B. Fischer, Phys. Rev. E **70**, 046108 (2004).
[28] A. Gordon and B. Fischer, Opt. Lett. **29**, 69 (2004).
[29] R. Weill, A. Rosen, A. Gordon, O. Gat, and B. Fischer, Phys. Rev. Lett. **95**, 013903 (2005).
[30] M. Katz, A. Gordon, O. Gat, and B. Fischer, Phys. Rev. Lett. **97**, 113902 (2006).
[31] B. Vodonos, A. Bekker, V. Smulakovsky, A. Gordon, O. Gat, N. K. Berger, and B. Fischer, Opt. Lett. **30**, 2787 (2005).
[32] R. Gordon, Omri Gat, B. Fischer, and F. X. Krtner, Opt. Express **14**, 11142 (2006).
[33] H. E. Stanley, *Introduction to Phase Transitions and Critical Phenomena* (Oxford University Press, New York, 1971).
[34] Ö Illday, Ph.D. dissertation, Cornell University, 2004 (unpublished).
[35] K. Smith, N. J. Doran, and P. G. J. Wigley, Opt. Lett. **15**, 1294 (1990).
[36] H. Haken, in *Laser Handbook*, edited by F. T. Arecchi and E. O. Schulz-Dubois (North-Holland, Amsterdam, 1972), Vol. 1, pp. 115–150.
[37] H. Haken, *Synergetics*, 2nd ed. (Springler-Verlag, Berlin, 1989).
[38] H. Risken, *The Fokker-Planck Equation*, 2nd ed. (Springer-Verlag, Berlin, 1989).
[39] H. A. Haus and A. Mecozzi, IEEE J. Quantum Electron. **29**, 983 (1993).
[40] J. Maunuksela, M. Myllus, J. Merikoski, J. Timonen, T. Kärkkäinen, M. S. Welling, and R. J. Wijngaarden, Eur. Phys. J. B **33**, 193 (2003).